ORGANOMETALLICS

Rhodium Complexes with a Pyridine-2-yloxy-silyl-Based N,Si-Ligand: Bonding Situation and Activity as Alkene Hydrogenation Catalysts

Alejandra Gómez-España, Pilar García-Orduña, Fernando J. Lahoz, Israel Fernández,* and Francisco J. Fernández-Álvarez*

Cite This: *Organometallics* 2024, 43, 402−413 Read Online

ABSTRACT: Rh(III) complexes [Rh(H)(X)(κ^2-NSi^{tBu2OPy})(L)] (X = Cl, L = PCy$_3$, **2a**; PH^{t}Bu$_2$, **2b**; X = OTf, L = PCy$_3$, **3a**; PH^{t}Bu$_2$, **3b**) (NSi^{tBu2OPy} = 4-methylpyridin-2-yloxy-ditertbutylsilyl) have been prepared and characterized by means of elemental analysis and nuclear magnetic resonance (NMR) spectroscopy. The solid-state structures of complexes **2a**, **2b**, and **3a** have been determined by X-ray diffraction studies. Computational analyses of the bonding situation of these species evidence the electron-sharing nature of the Rh−Si bond and the significant role of the electrostatic component in the interaction between the transition metal fragment [Rh(H)(PR$_3$)(X)]$^\bullet$ and the [NSi^{tBu2OPy}]$^\bullet$ ligand. In addition, a comparative study of the activity of **2a**, **2b**, **3a**, **3b**, and related iridium species as catalysts for the hydrogenation of olefins has been performed. The best catalytic results have been obtained when using the Rh(III) species **3a**, with triflate and PCy$_3$ ligands, as catalyst. Computational density functional theory studies show that the formation of the alkane is thermodynamically favored and that the rate-limiting step corresponds to the hydrogen activation, which takes place via a σ-complex-assisted metathesis mechanism.

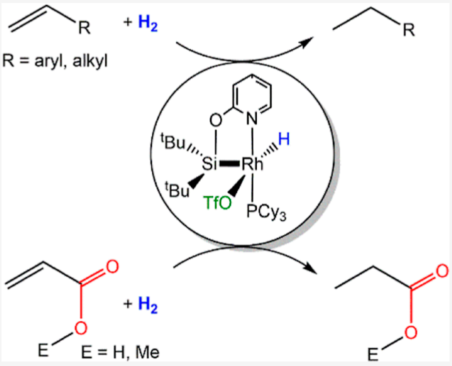

INTRODUCTION

The chemistry of transition metal (TM) complexes with tetradentate κ^4-L$_3$Si, tridentate κ^3-L$_2$Si and/or bidentate κ^2-LSi ligands—where Si symbolizes a silyl group and L phosphine ligands,[1−3] *N*-heterocycles,[4] *N*-heterocyclic carbenes (NHCs),[5] or thioether groups[6,7]—is growing in interest. The electronic and steric properties of multidentate organosilyl ligands are easily tunable by changing the substituents at the silicon and donor (L) groups. Moreover, their strong σ-donating ability and the high trans-influence of the silicon atom facilitate the formation of coordinatively unsaturated TM complexes.[1−7] Most of the studies on TM complexes with multidentate silyl ancillary ligands published to date are focused on the chemistry of species with tridentate ligands of type κ^3-L$_2$Si, which have been the subject of numerous reviews in recent years. In this regard, it should be mentioned that the chemistry of the TM complexes with bidentate κ^2-PSi,[3] κ^2-NSi,[4b] κ^2-(NHC)Si,[5] or κ^2-SSi[7] ligands, which by comparison has been less explored, is gaining attention in recent years. Among them, κ^2-NSi ligands stand out for being easy to prepare, tunable, versatile, and relatively low cost.

Our group has recently focused on studying the potential of iridium complexes with bidentate pyridine-2-yloxy-silyl-based ligands κ^2-(NSi^{R2OPy}) as homogeneous catalysts. The strength and chemical inertness of the metal−silicon bond in TM complexes with κ^2-(NSi^{R2OPy}) ligands differ from what would be expected for a traditional metal−silyl bond.[8−16] Initially, the metal−Si bonds in TM-{κ^2-(NSi^{R2OPy})} species were proposed as base-stabilized metal-silylenes.[9−11] However, in 2020, it was demonstrated that their metal-silyl character could not be ruled out.[12] Indeed, recent studies have shown that the Ir−Si bonds in Ir-{κ^3-(NSiN)}[13] and Ir-{κ^2-(NSi^{R2OPy})}[14] complexes can be described as highly polarized covalent Ir−silyl bonds with a significant electrostatic component, which can be even stronger than the sum of the orbital interactions.

The steric hindrance of the substituents around the silicon atom plays an important role in the reactivity and structure of Ir-{κ^2-(NSi^{R2OPy})} species. Thus, while in iridium(III) complexes with 4-methylpyridin-2-yloxy-dimethylsilyl (κ^2-NSi^{Me2OPy})[8] and 4-methylpyridin-2-yloxy-diisopropylsilyl (κ^2-NSi^{iPr2OPy})[12] ligands, the coordination of two ligand units to the metal center affording saturated iridium(III) species occurs very easily when using the 4-methylpyridin-2-yloxy-ditertbutylsilyl (κ^2-NSi^{tBu2OPy})[14,15] ligand, with tertbutyl instead of methyl or isopropyl substituents; only the coordination of one ligand unit is possible (Figure 1). In addition, the presence of the tertbutyl substituents at the silicon atom of Ir-(κ^2-

Received: December 1, 2023
Revised: January 8, 2024
Accepted: January 11, 2024
Published: January 23, 2024

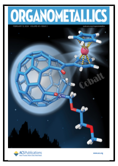

ACS Publications

https://doi.org/10.1021/acs.organomet.3c00498

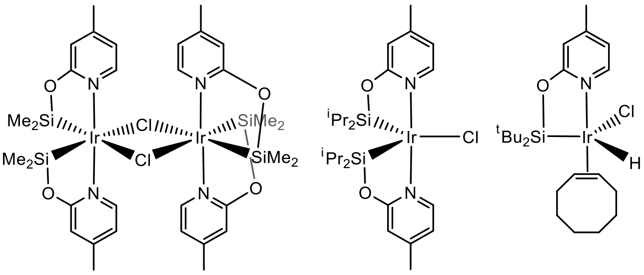

Figure 1. Examples of Ir-{κ^2-(NSi^{R2OPy})} (R = Me, ^{i}Pr, ^{t}Bu) species with pyridine-2-yloxy-silyl-based ligands.

NSi^{tBu2OPy}) species provides additional steric protection to the Ir−Si bond and allows the stabilization of unsaturated 16-electron square planar or bipyramidal trigonal iridium(III) species.[14,15]

The chemistry of rhodium with κ^2-(NSi^{R2OPy}) ligands has been poorly studied in comparison to that of iridium. In 2019, we reported the first examples of Rh-{κ^2-(NSi^{Me2OPy})}$_2$ complexes (Figure 2). These species have proven to be efficient catalyst precursors for the formation of silylcarbamates from the reaction of CO$_2$ with hydrosilanes and secondary amines.[16] A few examples of rhodium(III) complexes with other types of monoanionic κ^2-Si,N ligands have been recently described.[17,18] So, Huertos et al. have reported that the ligands 8-(dimethylsilyl)quinoline (NSi^{Me2Q}), 8-(dimethylsilyl)-2-methylquinoline (NSi^{Me2QMe}) and 4-(dimethylsilyl)-9-phenylacridine (NSi^{Me2AC}) can be used successfully to prepare unsaturated Rh(III)-{κ^2-(NSi^{Ar})} (NSi^{Ar} = NSi^{Me2Q}, NSi^{Me2QMe}, NSi^{Me2AC}) species,[17] and Komuro, Hashimoto et al. have reported rhodium complexes with a κ^2-(N,Si)-silyl-1,8-naphthyridine ligand "κ^2-(*naphySi*)" (Figure 2).[18]

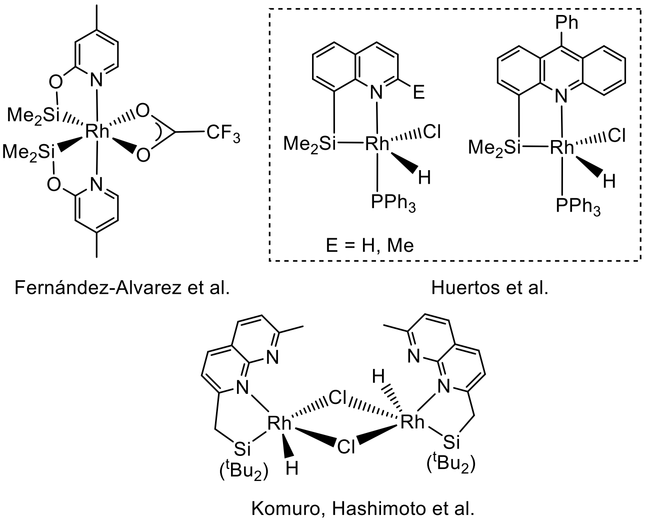

Figure 2. Examples of Rh-{κ^2-(NSi)} species previously reported.

Considering the above-commented precedents, and particularly, the scarcity of studies devoted to the chemistry of rhodium complexes featuring κ^2-N,Si ligands, in this work, we have explored first the potential of the monoanionic bidentate NSi^{tBu2OPy} ligand, with tertbutyl substituents at the silicon atom to stabilize unsaturated Rh-{κ^2-(NSi^{tBu2OPy})} active species, to then investigate the performance of these species as catalysts for the hydrogenation of alkenes.

RESULTS AND DISCUSSION

Synthesis and Characterization of Rh-(κ^2-NSi^{tBu2OPy})(PR$_3$) Complexes. The reaction of the functionalized silane (4-methyl-pyridin-2-yloxy)ditertbutylsilane (**1**, NSi^{tBu2OPy}-H) with [Ir(Cl)(coe)$_2$]$_2$ (coe = *cis*-cyclooctene), which quantitatively leads to the formation of the iridium(III) species [Ir(H)(Cl)(κ^2-NSi^{tBu2OPy})(coe)] as shown in Figure 1,[15a] has been key to developing the chemistry of Ir-{κ^2-(NSi^{tBu2OPy})} derivatives. However, this methodology is not applicable in the case of rhodium as the desired species [Rh(H)(Cl)(κ^2-NSi^{tBu2OPy})(coe)] was never obtained when the analogous reaction was performed using [Rh(Cl)(coe)$_2$]$_2$ as the metallic precursor, regardless of the stoichiometry. Instead, the formation of mixtures of unidentified rhodium complexes and free coe was observed. Therefore, to stabilize the possible Rh-{κ^2-(NSi^{tBu2OPy})} intermediates generated during the reaction of **1** with [Rh(Cl)(coe)$_2$]$_2$, we decided to perform the reaction in the presence of PCy$_3$ (or PH^{t}Bu$_2$). To our delight, the reaction of [Rh(Cl)(coe)$_2$]$_2$ with 1 equiv of **1** per rhodium and in the presence of stoichiometric amounts of PCy$_3$ (or PH^{t}Bu$_2$) at 273 K quantitatively afforded the corresponding rhodium(III) complexes [Rh(H)(Cl)(κ^2-NSi^{tBu2OPy})(L)] (L = PCy$_3$, **2a**; PH^{t}Bu$_2$, **2b**) (Scheme 1), which were isolated as bright yellow solids in 91 and 96% yield, respectively. Treatment of light-protected toluene solutions of **2a** (or **2b**) with 1 equiv of AgOTf affords the corresponding compounds [Rh(H)(OTf)(κ^2-NSi^{tBu2OPy})(L)] (L = PCy$_3$, **3a**; PH^{t}Bu$_2$, **3b**). Complexes **3a** and **3b** were isolated as an off-white (**3a**) or a light brown (**3b**) solid, in 84 and 79% yield, respectively (Scheme 1).

Scheme 1. Preparation of Rh-{κ^2-(NSi^{tBu2OPy})} Complexes

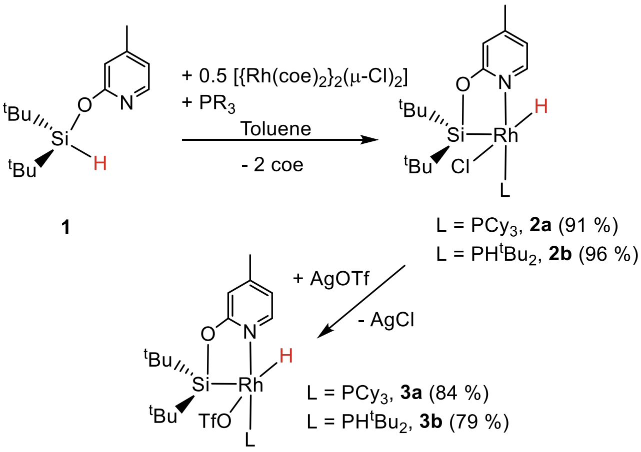

Complexes **2a**, **2b**, **3a**, and **3b** have been characterized by means of elemental analysis, nuclear magnetic resonance (NMR) spectroscopy, and high-resolution mass spectrometry (HR-MS) (Figures S1−S30). The most noticeable resonance in the proton NMR (^{1}H NMR) spectra of the Rh-PCy$_3$ derivatives **2a** and **3a** in C$_6$D$_6$ is a double doublet at δ −17.22 ppm ($^1J_{H-Rh} \approx 26$ Hz, $^2J_{H-P} \approx 20$ Hz) and −21.72 ppm ($^1J_{H-Rh} \approx 33$ Hz, $^2J_{H-P} \approx 22$ Hz), respectively, which confirms the presence of a Rh−H bond in both species. The ^{1}H NMR spectra of the Rh-PH^{t}Bu$_2$ species **2b** and **3b** show the resonance due to the Rh−H bond as a doublet of doublets of doublets (ddd) centered at δ −18.20 ppm ($^1J_{H-Rh} \approx 28.8$ Hz, $^2J_{H-P} \approx 19.8$ Hz, $^3J_{H-H} \approx 4.6$ Hz) and −22.18 ppm ($^1J_{H-Rh} \approx$

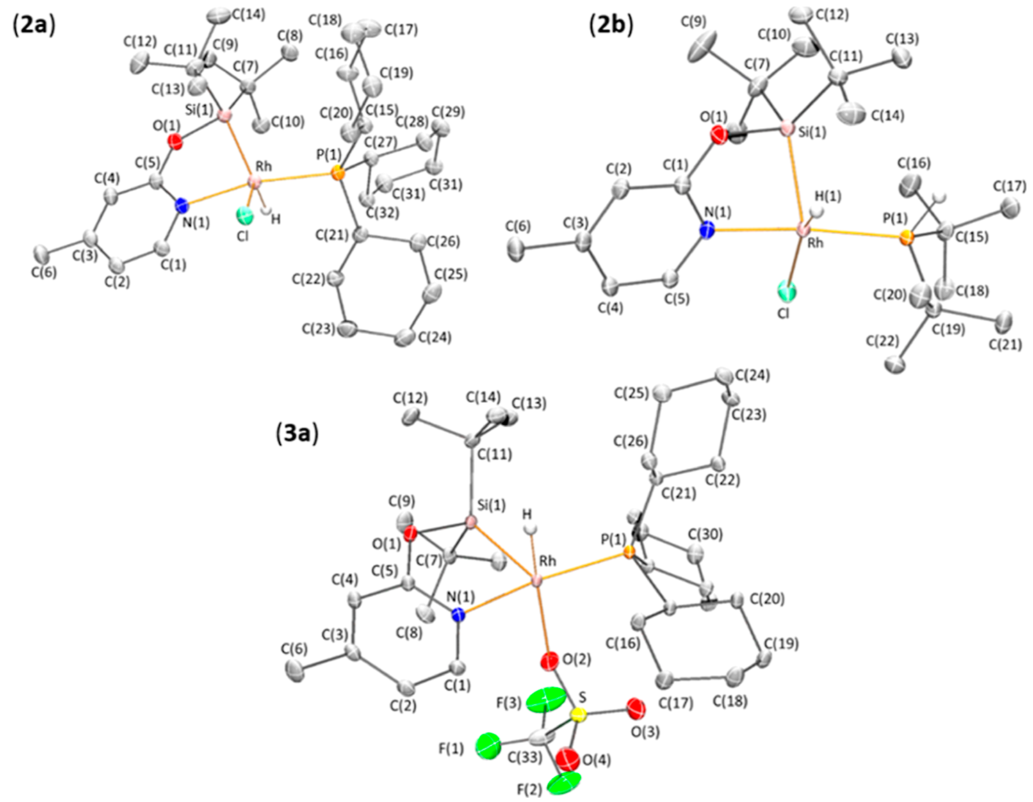

Figure 3. Molecular structures of complexes **2a**, **2b**, and **3a**. Hydrogen atoms (except hydrides and those of P−H fragments) have been omitted for clarity.

33.3 Hz, $^2J_{H-P}$ ≈ 21.5 Hz, $^3J_{H-H}$ ≈ 3.9 Hz). In addition, the proton corresponding to the P−H moiety also appears as a ddd centered at δ 4.39 ppm ($^1J_{H-P}$ ≈ 329 Hz; $^2J_{H-Rh}$ ≈ $^3J_{H-H}$ ≈ 4.6 Hz; **2b**) and 4.10 ppm ($^1J_{H-P}$ ≈ 340 Hz; $^2J_{H-Rh}$ ≈6.1 Hz; $^3J_{H-H}$≈ 3.9 Hz; **3b**), respectively. The ^{29}Si{^{1}H} NMR spectra show a double doublet resonance at δ 83.3 ppm ($^1J_{\mathrm{Si-Rh}}$ ≈ 35 Hz, $^2J_{\mathrm{Si-P}}$ ≈ 9 Hz; **2a**), 78.7 ppm ($^1J_{\mathrm{Si-Rh}}$ ≈ 30 Hz, $^2J_{\mathrm{Si-Rh}}$ ≈ 9 Hz; **2b**), 87.9 ppm ($^1J_{\mathrm{Si-Rh}}$ ≈ 40 Hz, $^2J_{\mathrm{Si-P}}$ ≈ 9 Hz; **3a**), and 85.9 ppm ($^1J_{\mathrm{Si-Rh}}$ ≈ 36 Hz, $^2J_{\mathrm{Si-P}}$ ≈ 9 Hz; **3b**). Therefore, the ^{29}Si chemical shift observed for complexes **2a**, **b** and **3a**, **b** (in the range of δ 78.7−87.9 ppm) is clearly low-field shifted in comparison with the ^{29}Si resonances (δ 41.2−50.7 ppm), recently reported for neutral Rh(III)-(κ^2-NSi$^{\mathrm{Ar}}$) (NSi$^{\mathrm{Ar}}$ = NSi$^{\mathrm{Me2Q}}$, NSi$^{\mathrm{Me2QMe}}$, NSi$^{\mathrm{Me2AC}}$) species (Figure 2),[17] but compares well with the value of 79.4 ppm found for Rh-{κ^2-(*naphySi*)} species (Figure 2).[18] The $^1J_{\mathrm{Rh-Si}}$ values found for complexes **2a** (35 Hz), **2b** (30 Hz), **3a** (42 Hz), and **3b** (41 Hz) confirm the silyl character of the Rh−Si bond[19] and compare well with those observed in the ^{29}Si{^{1}H} NMR spectra of [Rh(X)(κ^2-NSi$^{\mathrm{Me2OPy}}$)$_2$] species (X = Cl, δ 85.7 ppm, $^1J_{\mathrm{Si-Rh}}$ ≈ 37 Hz; X = κ^2-O_2CCF_3, δ 86.2 ppm, $^1J_{\mathrm{Si-Rh}}$ ≈ 39 Hz).[16] Moreover, their phosphorus-31 NMR (^{31}P{^{1}H} NMR) spectra (C_6D_6) exhibit a doublet at δ 46.4 ppm ($^1J_{\mathrm{P-Rh}}$ ≈ 142.0 Hz; **2a**), δ 58.7 ppm ($^1J_{\mathrm{P-Rh}}$ ≈ 142.5 Hz; **2b**), δ 44.5 ppm ($^1J_{\mathrm{P-Rh}}$ ≈ 140.0 Hz; **3a**), and δ 55.7 ppm ($^1J_{\mathrm{P-Rh}}$ ≈ 141.1 Hz; **3b**).

The solid-state structures of **2a**, **2b**, and **3a** have been determined by single-crystal X-ray diffraction. As illustrated in Figure 3 and pointed out in Table 1, the geometry of the metal coordination sphere of the pentacoordinated complexes is independent of the phosphine ligand, contrary to the situation observed in iridium-analogous complexes.[14,15a] Thus, complex **2a**, with PCy$_3$, shows a distorted trigonal bipyramidal rhodium atom with the nitrogen and phosphorus atoms at apical positions and equatorial sites occupied by silicon, chloro, and hydrogen atoms. As shown in the Supporting Information (Figure S31), the relative disposition between Cl and hydride ligands, and the orientation of a ^{t}Bu group coordinated to the silicon atom differ from those observed in the iridium complex counterpart, which exhibits a square pyramidal geometry.

Table 1. Selected Bond Lengths (Å) and Angles (deg) for Complexes 2a, 2b, and 3a

	2a	2b	3a
Rh−X^a	2.4251(5)	2.4128(3)	2.2317(8)
Rh−P(1)	2.2810(5)	2.2538(3)	2.2896(3)
Rh−Si(1)	2.2907(6)	2.2738(3)	2.2689(3)
Rh−N(1)	2.1187(17)	2.1222(9)	2.0907(8)
Rh−H	1.52	1.501(17)	1.439(19)
X^a−Rh−P(1)	90.885(18)	94.635(11)	90.76(2)
X^a−Rh−Si(1)	133.34(2)	137.656(12)	112.73(3)
X^a−Rh−N(1)	88.23(5)	91.32(3)	89.55(3)
X^a−Rh−H	128.1	158.9(6)	175.0(7)
P(1)−Rh−Si(1)	109.36(2)	103.662(11)	112.033(9)
P(1)−Rh−N(1)	167.68(5)	167.56(3)	167.07(2)
P(1)−Rh−H	87.4	82.2(7)	88.5(8)
Si(1)−Rh−N(1)	79.84(5)	78.82(3)	79.65(2)
Si(1)−Rh−H(1)	95.4	62.8(6)	72.1(7)
N(1)−Rh−H(1)	83.5	88.3(7)	90.1(8)

On the other hand, in complexes **2b** and **3a**, with PH^{t}Bu$_2$ and PCy$_3$ ligands, respectively, the coordination of the κ^2-NSi$^{t\mathrm{Bu2OPy}}$ ligand through the N and Si atoms, together with that of the phosphorus, the hydride, and chloride (**2b**) or an oxygen atom of a triflate ligand (**3a**), leads to a distorted square pyramidal geometry around the rhodium atom, with the silicon atom in the apical position and the chloride (**2a**) or the oxygen atom of the triflate ligand (**3a**) located trans to the hydride [τ = 0.14 (**2b**), 0.17 (**3a**), 0.66 (**2a**)].[20]

The Rh−Si bond lengths [2.2907(6) Å, **2a**; 2.2738(3) Å, **2b**; 2.2689(3) **3a**] in the three complexes are found to be longer than those reported for the complex [Rh(κ^2-O_2CCF_3)(κ^2-NSi^{Me2OPy})$_2$] [2.2277(8) and 2.2388(10) Å],[16] an octahedral complex where the Si atom was located trans to oxygen atoms of the (κ^2-O) coordinated carboxylate ligand (Figure 3).

Computational Studies on the Rh−Si Bond in Complexes 2a and 2b and 3a and 3b. We have recently explored the nature of the Ir−Si bond in Ir-{*fac*-κ^3-(NSiN)}[13] and Ir-{κ^2-($NSi^{tBu2OPy}$)}[14] species. These studies showed that in both cases, the electrostatic component of the bond is almost twice as strong as the total orbital interactions, which indicates the occurrence of a highly polarized covalent bond.

To study the influence of the nature of the transition metal on the bonding situation and to explain the unexpected low field shift observed for the silicon atom in the ^{29}Si NMR spectra of complexes **2a**, **2b**, **3a**, and **3b**, we decided to investigate the Rh−Si bond in these complexes by means of computational tools. To this end, we applied state-of-art methods based on energy decomposition analysis (EDA) in combination with the natural orbital for chemical valence (NOCV) approach on these complexes at the relativistic and dispersion-corrected ZORA-BP86-D3/TZ2P//BP86-D3/def2-SVP level (see computational details in the Supporting Information), to enable a direct comparison with the data reported previously by us for the related Ir−Si species.[14]

According to the data in Table 2, the interaction energy (ΔE_{int}) between the [$NSi^{tBu2OPy}$]$^\bullet$ and [Rh(H)(PR_3)(X)]$^\bullet$ fragments is relatively high (ranging from ca. −121 to −128 kcal mol^{-1}), which indicates a strong bond between the selected fragments. The main contribution to the total interaction (ΔE_{int}) comes, in all cases, from the electrostatic attractions (ΔE_{elstat}), which represent ca. 56% of the total attractive interactions and are significantly stronger than the orbital interactions (ΔE_{orb}, contributes ca. 37% to the total bonding). At variance, the stabilizing interactions coming from dispersion forces (ΔE_{disp}) are comparatively much weaker (ca. 6.5% to the total bonding) yet not negligible. These results compare well with those obtained for related Ir-(κ^2-($NSi^{tBu2OPy}$)[14] species with values of around 58, 37, and 5% for the ΔE_{elstat}, ΔE_{orb}, and ΔE_{disp} components, respectively.[14]

Table 2. EDA-NOCV Results (in kcal mol^{-1}) Data for Complexes 2a, 2b, 3a, and 3b Computed at the ZORA-BP86-D3/TZ2P//BP86-D3/def2-SVP Level[a]

	2a	2b	3a	3b
ΔE_{int}	−123.3	−121.3	−127.9	−123.5
ΔE_{Pauli}	273.5	269.6	268.6	259.6
ΔE_{elstat}	−220.2	−222.2	−222.0	−215.7
ΔE_{orb}	−149.6	−147.7	−144.6	−141.1
$\Delta E(\rho_1)$ (σ-Rh−Si)	−82.3	−84.3	−79.0	−79.6
$\Delta E(\rho_2)$ (LP(N) → d(Ir))	−22.4	−21.8	−23.3	−23.0
$\Delta E(\rho_3)$ (d(Rh)→σ^*(Si−O))	−11.1	−11.5	−10.7	−9.7
ΔE_{disp}	−27.0	−21.0	−29.9	−26.3

[a] ΔE_{int} = ΔE_{elstat} + ΔE_{Pauli} + ΔE_{orb} + ΔE_{disp} (the Supporting Information).

However, it should be mentioned that the interaction between the [$NSi^{tBu2OPy}$]$^\bullet$ and [Ir(H)(PR_3)(X)]$^\bullet$ fragments is stronger (ranging from ca. −142 to −159 kcal mol^{-1})[14] than that found for rhodium (from ca. −121 to −128 kcal mol^{-1}), which indicates that the Rh−Si bonds in these species are comparatively weaker than the Ir−Si bonds in the Ir-(κ^2-($NSi^{tBu2OPy}$) complexes, suggesting that the trans influence exerted by the silicon atom should be slightly lower in rhodium complexes than in iridium complexes.

According to the NOCV method, the main orbital interactions between the [$NSi^{tBu2OPy}$]$^\bullet$ and [Rh(H)(PR_3)(X)]$^\bullet$ fragments in these Rh−Si species are composed of a covalent (i.e., electron-sharing) Rh−Si bond together with a dative LP(N) → Rh bond [where LP(N) refers to the nitrogen lone pair]. From the data in Table 2, the covalent Rh−Si bond (denoted as ρ1, Figure 4) is almost 4-fold stronger than the dative bond involving the donation from the lone pair of the pyridine nitrogen atom to a vacant d atomic orbital of the transition metal (denoted as ρ2). Similar to their Ir counterparts,[14] there also exists a weak yet noticeable π-backdonation from a doubly occupied d atomic orbital of the rhodium center to a σ^*(Si−O) molecular orbital (denoted as ρ3, Figure 4), whose strength is markedly much lower than that associated with the ρ1 or ρ2 orbital interactions (see Table 2). Therefore, our calculations indicate that these novel Rh-(κ^2-$NSi^{tBu2OPy}$) complexes feature a significant electrostatic attraction between the [$NSi^{tBu2OPy}$]$^\bullet$ and [Rh(H)(PR_3)(X)]$^\bullet$

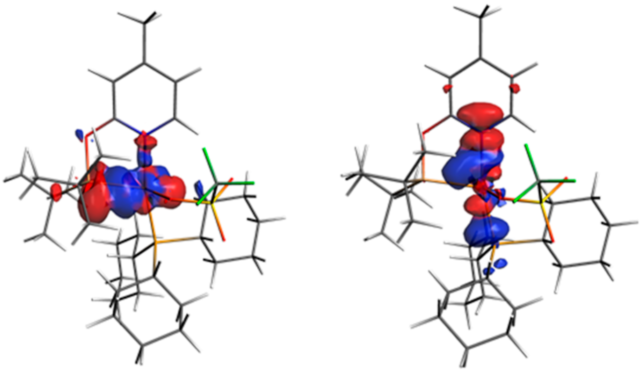

Si-Rh covalent bond
$\Delta E(\rho 1)$ = -79.0 kcal/mol

LP(N) to Rh dative bond
$\Delta E(\rho 2)$ = -23.3 kcal/mol

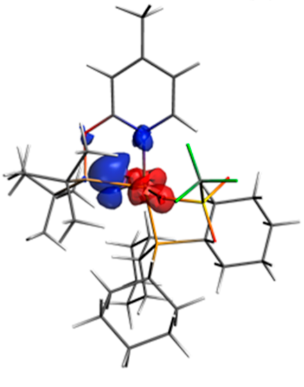

d(Rh) to π^*(Si) backdonation
$\Delta E(\rho 3)$ = -10.7 kcal/mol

Figure 4. NOCV-deformation densities and associated stabilization energies computed for complex **3a**. The charge flow takes place in the direction red → blue. All data have been computed at the ZORA-BP86-D3/TZ2P//BP86-D3/def2-SVP level.

fragments while the orbital component is mainly dominated by a covalent Rh−Si bond and, albeit to a lesser extent, by a dative LP(N) → Rh bond.

[RhH(X)(κ^2-NSi^{tBu2OPy})(L)] (X = Cl, OTf; L = PCy_3 or PH^tBu_2)-Catalyzed Hydrogenation of Alkenes. It has been recently proved that rhodium and iridium complexes with multidentate silyl ligands such as pincer-type Rh-{κ^3-(PSiP)}[21] species and iridium complexes with a silyl-1,8-naphthyridene-based Si,N-ligand[22] are active catalysts for the hydrogenation of alkenes. In this regard, during our studies on the potential of Ir-{κ^2-(NSi^{R2OPy})}[8c,15b,c] derivatives as catalysts precursors for the dehydrogenation of formic acid, we found that in the absence of the base (NEt_3 or NaOOCH), the metal−silicon bond in these species is stable under moderate H_2 pressure (1−5 bar). ^{1}H NMR studies of C_6D_6 solutions of the rhodium complexes **2a**, **2b**, **3a**, and **3b** showed that these species are also stable in the presence of H_2 (5 bar) even at 353 K. These results motivated us to study the potential of Ir- and Rh-{κ^2-(NSi^{tBu2OPy})} complexes as hydrogenation catalysts.

A comparative study of the activity of the rhodium complexes **2a**, **2b**, **3a**, and **3b**, and the iridium species [Ir(H)(OTf)(κ^2-NSi^{tBu2OPy})(L)] (L = PCy_3 **4a**; PH^tBu_2, **4b**; Figure 5)[14] as catalysts (5 mol %) for the reaction of styrene with H_2 (5 bar) in C_6D_6 at 353 K, in the presence of hexamethylbenzene as internal standard, shows that the catalytic performance depends on both the metal and on the ancillary ligand (Cl or OTf) (Table 3). In all cases, after 3 h of reaction, the selective formation of ethylbenzene was observed. The higher activities were obtained when using the rhodium-triflate derivatives **3a** (100%) and **3b** (90%) (Table 3). It should be mentioned that under the same reaction conditions, the catalytic systems based on the related iridium species **4a** and **4b** showed a comparatively lower catalytic performance (Table 3, entries 5 and 6), which could be ascribed to the higher trans influence exerted by the Ir−Si bond in comparison with that by the Rh−Si bond.

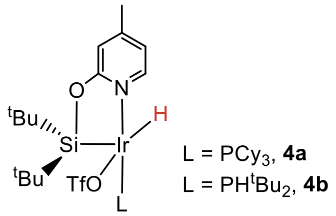

Figure 5. Complexes **4a** and **4b**.

Table 3. Results from the Rh- and Ir-NSi^{tBu2OPy}-Catalyzed Hydrogenation of Styrene[a]

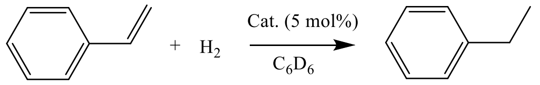

entry	catalyst	metal	ethylbenzene (%)[b]
1	**2a**	Rh	86
2	**2b**	Rh	81
3	**3a**	Rh	>99
4	**3b**	Rh	90
5	**4a**	Ir	44
6	**4b**	Ir	16

[a] The reactions were performed in C_6D_6 at 353 K using 5 mol % of catalyst and in the presence of hexamethylbenzene as internal standard. [b] Based on the ^{1}H NMR integral, after 3 h, all the reactions are selective to ethylbenzene.

These results show that **3a** is slightly more active, under the studied reaction conditions, than **2a**, **2b**, **3b**, **4a**, and **4b**. Therefore, we decided to perform *Operando* ^{1}H NMR studies of the **3a**-catalyzed reaction of styrene with H_2 at different hydrogen pressures and temperatures. Thus, we studied the effect of reducing the H_2 pressure from 5 to 2.5 bar. The **3a**-catalyzed (5 mol %) reaction of styrene with H_2 (5 bar) at 353 K requires 25 min to achieve the full conversion of styrene into ethylbenzene; however, under 2.5 bar of H_2, 35 min was required. Therefore, at 353 K, a reduction of the H_2 pressure from 5 to 2.5 bar produces a slight decrease in activity, which is not significant (Figure S33). At this point, we decided to study the effect of temperature on the **3a**-catalyzed (5 mol %) reactions of styrene with H_2 (5 bar). Thus, the catalytic reactions were monitored by ^{1}H NMR at different temperatures. The results of these studies show that there is a clear effect of the temperature, with a gradual increase in activity from 333 to 353 K (Figures S34−S36). The Arrhenius plot for these data yields an apparent activation energy of 25.7 ± 0.4 kcal mol^{-1} (Figure S37).

^{1}H NMR studies of the **3a**-catalyzed (1.0 mol %) reaction of styrene with H_2 (5 bar) at 353 K show after 3 h a 65% conversion to ethylbenzene, a value clearly lower than that observed when using a 5 mol % of catalyst loading (100%, Table 3). Therefore, within the conditions studied, the optimal reaction conditions are 5 mol % of catalyst loading, 353 K, and 5 bar of H_2.

These results encouraged us to expand the scope of our study. To this end, we decided to limit the study to complexes **3a** and **3b** which proved to be the most active catalysts for the hydrogenation of styrene as compared to **2a**, **2b**, **4a**, and **4b**. Moreover, we have chosen different olefins such as 2-methyl-styrene, 3-methyl-styrene, *cis*-cyclooctene (*coe*), 1-pentene, *cis*-2-pentene, and functionalized alkenes such as methyl acrylate and 4-pentenoic acid. The results from these studies, which are gathered in Table 4, evidenced that both species are active in all the studied cases. The catalytic system based on **3a** allows the quantitative conversion to the corresponding hydrogenation product in most cases, apart from *coe*, which after 3 h was hydrogenated in only 87% to cyclooctane (Table 4, entry 5), which could be due to the high steric requirement of the Ir-cyclooctyl fragment.[23] Conversely, the system based on **3b** showed a poorer catalytic activity in the hydrogenation of 2-methylstyrene (47%, Table 4, entry 2) and *cis*-2-pentene (63%, Table 4, entry 10). In all the cases shown in Table 4, the selective hydrogenation of the olefin was observed, and neither alkene isomerization nor hydrogenation of aromatic rings or carboxylic groups were observed.

^{1}H NMR studies of the **3a**-catalyzed (5 mol %) reaction of (*Z*)-stilbene with H_2 (5 bar) in C_6D_6 at 353 K show the full conversion of the starting (*Z*)-stilbene into a mixture of the hydrogenation product $Ph(CH_2)_2Ph$ (≈65%) and (*E*)-stilbene (≈35%) after 3 h. Interestingly, when a similar reaction was performed using (*E*)-stilbene instead of (*Z*)-stilbene, the same result was obtained after 3 h of reaction. These results pointed to a **3a**-catalyzed (*Z*)-stilbene/(*E*)-stilbene isomerization prior to the hydrogenation. Furthermore, these results show that the hydrogenation of (*Z*)-stilbene is faster than the hydrogenation of (*E*)-stilbene. In agreement with that, it has been demonstrated that complex **3a** (5 mol %) catalyzes the

Table 4. Results from the **3a**- and **3b**-Catalyzed (5 mol %) Selective Hydrogenation (5 bar H_2) of Akenes in C_6D_6 at 353 K after 3 h[a]

Entry	Cat.	Substrate	Product	Yield (%)
1	**3a**	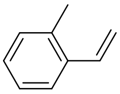	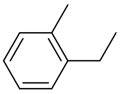	>99
2	**3b**	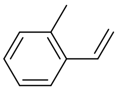	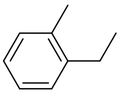	47
3	**3a**	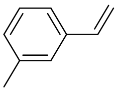	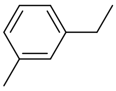	>99
4	**3b**	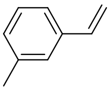	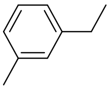	>99
5	**3a**	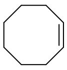	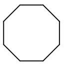	87
6	**3b**	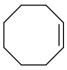	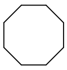	>99
7	**3a**	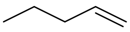	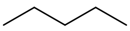	>99
8	**3b**	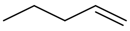	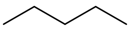	96
9	**3a**	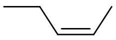	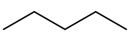	>99
10	**3b**	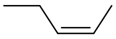	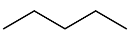	63
11	**3a**	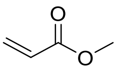	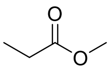	>99
12	**3b**	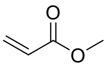	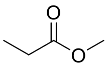	90
13	**3a**	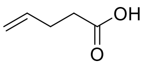	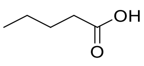	>99
14	**3b**	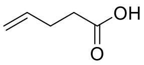	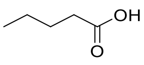	>99

[a]The reactions were done in the presence of hexamethylbenzene as internal standard.

isomerization of (*Z*)-stilbene to (*E*)-stilbene at 353 K to afford a mixture (*Z*)/(*E*) in a 3/97 ratio after 24 h (Figure S38), which can only be explained by a classical insertion/β-hydrogen elimination equilibrium. These results evidenced that the coordination of the olefin to **3a** and its subsequent reversible insertion into the Rh–H bond are very likely under the reaction conditions.

It should be mentioned that the *Operando* ^{1}H NMR studies of the **3a**-catalyzed reactions show that **3a** is the only rhodium species observed in the ^{1}H NMR spectra along the catalytic process. Moreover, solutions of **3a** at 353 K have proven to be stable in the presence of H_2 (5 bar), which confirms that under the reaction conditions, the possible oxidative addition of H_2 to **3a** to give a hypothetical rhodium(V) species does not take place.

In the search for evidence on the nature of the possible reaction intermediates, we performed ^{1}H NMR studies of the reaction of **3a** with 4 equiv of styrene in C_6D_6. These studies revealed that heating above 60 °C is necessary to observe a reaction. Under these conditions, the slow decomposition of **3a** into a mixture of unidentified complexes was observed. Remarkably, no new Rh–H resonances were observed, which suggests that the insertion of the styrene into the Rh–H bond of **3a** could take place during the reaction. However, the resulting Rh–CH_2CHPh[24] intermediate could not be identified under the reaction conditions.

Therefore, it can be concluded that **3a** is a versatile catalyst that promotes the hydrogenation of different types of olefins, such as linear olefins with aromatic and aliphatic substituents, cyclic olefins, and functionalized olefins. Despite that, its activity is lower than that published for related Ir-{κ^2-(*naphySi*)} species.[22]

Considering the above-commented experimental evidence, a plausible reaction mechanism for the **3a**-catalyzed hydrogenation of α-olefins is proposed in Scheme 2. It is reasonable to assume that the insertion of the α-olefin into the Rh–H bond constitutes the first step of the process affording a Rh-alkyl intermediate,[24] which is then stabilized by the coordination of a hydrogen molecule. We propose that the H_2 bond activation occurs via a σ-complex-assisted metathesis (σ-CAM) process,[25] which produces the corresponding alkane and regenerates **3a**.

Scheme 2. Proposed Mechanism for the **3a**-Catalyzed Hydrogenation of α-Alkenes

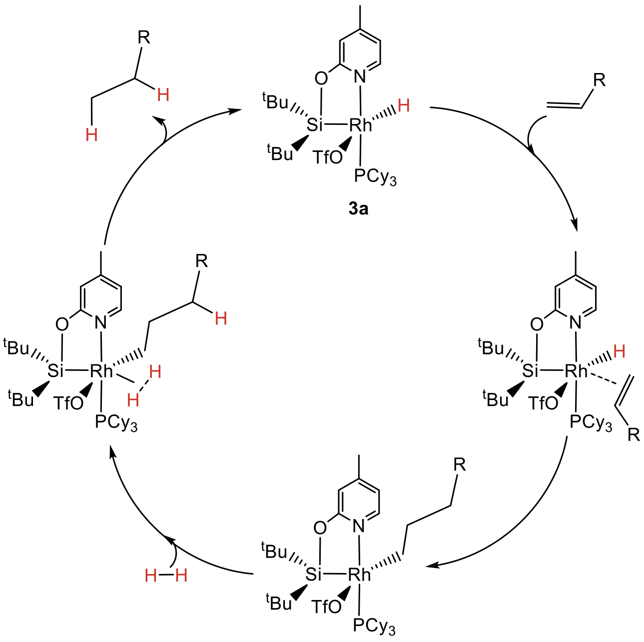

Further support for the above-proposed mechanism is given by the exploration of the transformation by computational tools. Figure 6 shows the computed reaction profile for the model reaction involving the hydrogenation of propene to propane mediated by the model catalyst **3M** (where the bulky ^{t}Bu and cyclohexyl groups in **3a** were replaced by methyl groups). As depicted in Figure 6, the process begins with the slightly endergonic (ΔG = 5.5 kcal mol^{-1}) coordination of the alkene to the coordination vacancy of the catalyst. Then, the insertion of the olefin into the Rh–H bond through the transition state **TS1** takes place, leading to the formation of the

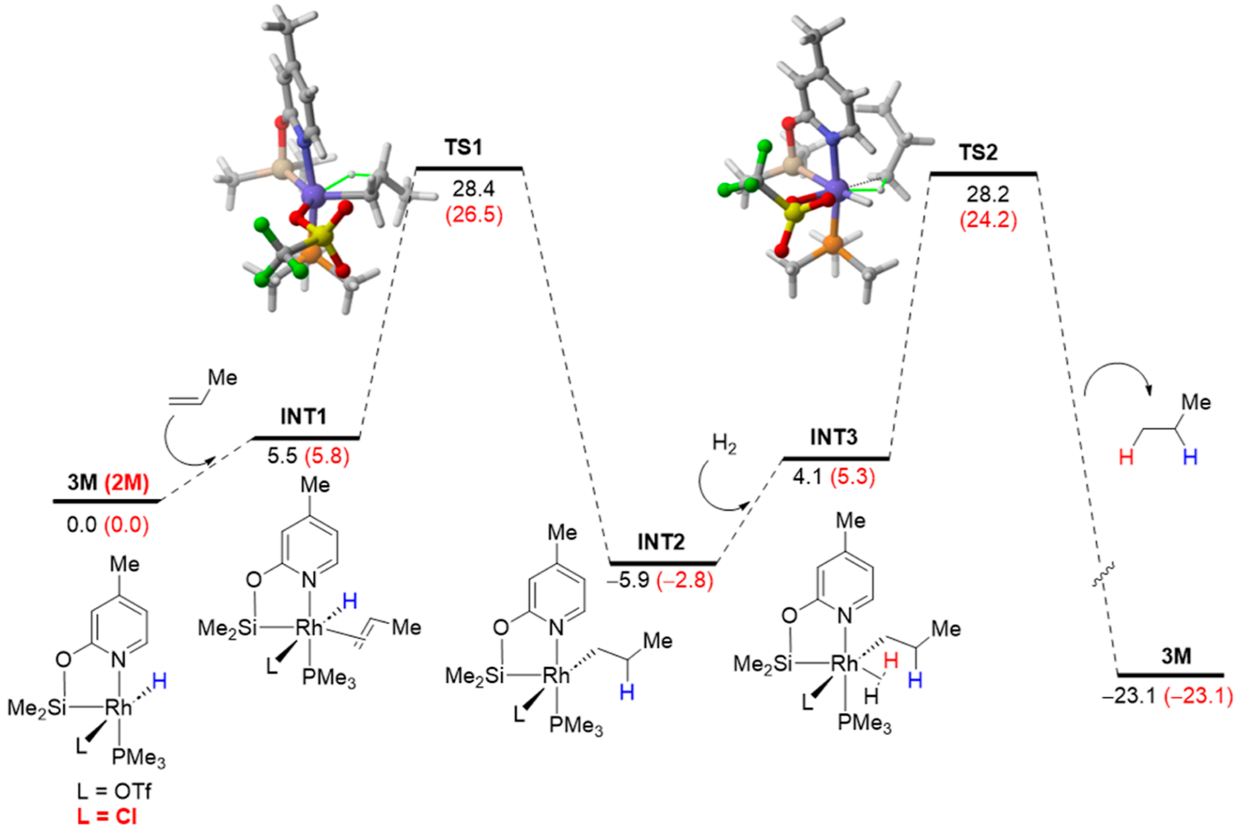

Figure 6. Computed reaction profile for the hydrogenation of propene catalyzed by **3M** (or **2M**). Relative free energies (ΔG, at 298 K) are given in kcal mol^{-1}. All data have been computed at the PCM (benzene)-BP86-D3/def2-SVP level.

Rh-alkyl intermediate **INT2**. The computed barrier of ca. 28 kcal mol^{-1} and exergonicity ($\Delta G = -5.9$ kcal mol^{-1}) of this step are compatible with the relatively high temperature used in the experiments (353 K) and with the value of 25.7 kcal mol^{-1} found for the apparent activation energy. Then, the new coordination vacancy in **INT2** is saturated by a molecule of H_2 forming the σ-complex **INT3**, again in an endergonic transformation, which finally evolves into the observed alkane with concomitant regeneration of the catalyst. The barrier associated with this final step (via **TS2**) compares to that computed for the initial insertion step and therefore is also compatible with the experimental conditions. The formation of the final alkane is highly exergonic ($\Delta G = -23.1$ kcal mol^{-1}), which compensates for the previous endergonic steps and drives the entire transformation forward. A rather similar reaction profile has been computed for the chloride analog **2M**. Therefore, activation of the Rh−Si bond does not occur during the catalytic process, which is in accordance with the strength of the Rh−Si bond described above.

Therefore, Rh-(κ^2-NSi^{tBu2OPy}) species **3a** is an efficient alkene hydrogenation catalyst. The rate-limiting step of the overall catalytic process is the H_2 activation via a σ-CAM (**TS2** in Figure 6). That contrasts with related, recently published Rh-[κ^3-P_2Si] species where the silyl-phosphine-based ligands stabilize low oxidation states, facilitating the H_2 activation by oxidative addition to Rh(I) species.[21] However, for rhodium or iridium species with κ^2-NSi-based ligands, low oxidation states, Rh(I) or Ir(I), are not favored, and therefore, Rh(I)/Rh(III) mechanisms are not favorable. Thus, the related Ir(III)-{κ^2-(*naphySi*)} species in which the Ir(I) oxidation state is not favorable either, the hydrogen activation process is reported to be assisted by the adjacent nitrogen lone pair.[22]

CONCLUSIONS

The one-pot reaction of the rhodium(I) complex [Rh(Cl)(coe)$_2$]$_2$ with the ligand precursor NSi^{tBu2OPy}-H (**1**) and the corresponding phosphine quantitatively affords the corresponding unsaturated species [Rh(H)(Cl)(κ^2-NSi^{tBu2OPy})(L)] (L = PCy$_3$, **2a**; PH^{t}Bu$_2$, **2b**), which reacts with 1 equiv of silver triflate to afford [Rh(H)(OTf)(κ^2-NSi^{tBu2OPy})(L)] (L = PCy$_3$, **3a** and PH^{t}Bu$_2$, **3b**). The solid-state structures of complexes **2a**, **2b**, and **3a** have been determined by X-ray diffraction studies. Computational analyses of the interaction between neutral [NSi^{tBu2OPy}]$^\bullet$ and [Rh(H)L(X)]$^\bullet$ fragments in **2a**, **2b**, **3a**, and **3b** confirm the electron-sharing nature of the covalent Rh−Si bond and the significant role of electrostatic attractions in the interaction between the transition metal fragment and the κ^2-NSi^{tBu2OPy} ligand. In addition, these studies indicate that the Rh−Si bonds in these species are comparatively weaker than the Ir−Si bonds in the related Ir-(κ^2-(NSi^{tBu2OPy}) complexes.

The activity of Rh- and Ir-{κ^2-(NSi^{tBu2OPy})} species as catalysts for the hydrogenation of α-olefins depends on both the metal and the ancillary ligand. The best catalytic performance has been obtained when using the rhodium−triflate complex **3a**, with PCy$_3$ ligand, as the catalyst at 353 K, which allows the quantitative and selective formation of the corresponding alkane in all the studied cases. It is notable that the metal−silicon bond in this type of complexes is stable under hydrogenation conditions, which opens the door to research on NSi ligand design in search of improved activity.

Computational studies show that the **2a**- and **3a**-catalyzed hydrogenation of alkenes can be viewed as a two-step process consisting of an initial insertion of the olefin in the Rh-hydride bond followed by a dihydrogen activation and release of the corresponding alkane by means of a σ-CAM reaction. After the olefin insertion into the Rh-hydride bond, the activation barriers for the reverse β-hydrogen elimination step and the forward hydrogenation processes are similar, but the **2a**- and **3a**-catalyzed hydrogenation of alkenes is thermodynamically driven.

Therefore, from the study of the nature of the bond, we can conclude that the Rh−Si bond is slightly weaker than the Ir−Si bond in the analogous iridium complexes. This implies that the silicon atom exerts a lower trans effect in rhodium species than that in iridium species and corresponds to the activity trend found when they are used as catalysts in olefin hydrogenation processes, where rhodium complexes with a lower trans effect have greater activity. On the other hand, the influence of the auxiliary ligands, chloride, triflate, and phosphine, on the catalytic activity is less relevant than the nature of the metal.

■ EXPERIMENTAL SECTION

General Information. All manipulations were performed with rigorous exclusion of air at an argon/vacuo manifold using standard Schlenk-tube or glovebox techniques. Solvents were dried by the usual procedures and distilled under argon prior to use. ^{1}H, ^{13}C{^{1}H}, ^{31}P{^{1}H}, ^{29}Si{^{1}H}, and ^{19}F{^{1}H} NMR spectra were recorded on a Bruker ARX, or Bruker Avance 300 MHz instrument. Chemical shifts (expressed in parts per million) are referenced to residual solvent peaks (^{1}H, ^{13}C{^{1}H}) and 85% H_3PO_4 (^{31}P{^{1}H}). Coupling constants J are given in hertz (Hz). Infrared spectra were recorded on a JASCO FT-IR 6600 spectrometer. (4-Methylpyridin-2-yloxy)-ditertbutylsilane[15a] and [{Rh(coe)$_2$}$_2$(μ-Cl)$_2$][26] were prepared following the reported methodology. The hydrogenation products were characterized by comparing their ^{1}H NMR spectra with the reported data (see Figures S39−S47).

Preparation of [Rh(H)(Cl)(κ^2-NSi^{tBu2OPy})(PCy$_3$)] (2a). Compound **1** (0.105 mL, 0.416 mmol) was added to a toluene suspension of [RhCl(coe)$_2$]$_2$ (0.15 g, 0.208 mmol) at 273 K. The resulting mixture was stirred at 273 K for 30 min. After that, a toluene solution (3.0 mL) of PCy$_3$ (0.117 g, 0.417 mmol) at 273 K was added, and the reaction mixture was warmed at room temperature and stirred overnight. The solvent was removed in vacuo, and the residue was washed with pentane (2 × 5 mL) and dried in vacuo to give a yellow powder of **2a** (253 mg, 91%). Anal. Calcd for $C_{32}H_{58}ClNOPRhSi$: C, 57.35; H, 8.72; N, 2.09. Found: C, 57.48; H, 8.78; N, 2.19. ^{1}H NMR plus HSQC ^{1}H−^{13}C, COSY ^{1}H−^{1}H and NOESY ^{1}H−^{1}H (300 MHz, 298 K, C_6D_6): δ 9.05 (dd, $^{3}J_{H-H} \approx 6.0$ Hz, $^{4}J_{H-P} \approx 2.7$ Hz, 1H, py-H^{6}), 6.32 (s, 1H, py-H^{3}), 6.09 (pseudo-d, $^{3}J_{H-H} \approx 6.0$ Hz, 1H, py-H^{5}), 2.45 (m, 3H, CH-PCy$_3$), 2.23 (m, 6H, CH_2-PCy$_3$), 1.77 (m, 12H, CH_2-PCy$_3$), 1.64 (m, 2H, CH_2-PCy$_3$), 1.60 (s, 3H, CH_3-py), 1.43 (s, 18H, CH_3-^{t}Bu), 1.26 (m, 16H, CH_2-PCy$_3$), −17.22 (dd, $^{1}J_{Rh-H} \approx 26$ Hz, $^{2}J_{H-P} \approx 20$ Hz, 1H, Rh−H). ^{13}C{^{1}H} APT plus HSQC ^{1}H−^{13}C (75 MHz, 298 K, C_6D_6): δ 165.5 (d, $^{2}J_{Rh-C} \approx 1.9$ Hz, py-C^{2}), 151.9 (s, py-C^{4}), 149.0 (s, py-C^{6}), 117.6 (s, py-C^{5}), 110.4 (s, py-C^{3}), 37.1 (d, $^{1}J_{P-C} = 21.6$ Hz, CH-PCy$_3$), 32.0 (s, 2C, Si−C(CH$_3$)$_3$), 31.0 (s, 6C, CH$_3$-^{t}Bu), 30.7 (s, 6C, CH$_2$−PCy$_3$), 28.0 (d, $^{2}J_{P-C} \approx 10.0$ Hz, 6C, CH$_2$−PCy$_3$), 26.9 (s, 3C, CH$_2$−PCy$_3$), 20.5 (s, CH$_3$-py). ^{31}P{^{1}H} NMR (121 MHz, 298 K, C_6D_6): δ 46.4 (d, $^{1}J_{\mathrm{Rh-P}} \approx 142$ Hz, Rh−P). ^{29}Si{^{1}H} NMR (60 MHz, 298 K, C_6D_6) plus HMBC ^{1}H−^{29}Si: δ 83.3 (dd, $^{1}J_{\mathrm{Rh-Si}} = 35.0$ Hz, $^{2}J_{\mathrm{P-Si}} = 9.0$ Hz, Rh−Si). High-resolution mass spectrometry (HR-MS) (ESI$^+$, m/z): calcd for $C_{32}H_{58}NOPRhSi$, $[M - Cl]^+$ 634.3080; found, 634.3105.

Preparation of [Rh(H)(Cl)(κ^2-NSi^{tBu2OPy})(PH^{t}Bu$_2$)] (2b). Compound **1** (0.244 mL, 0.972 mmol) was added to a toluene suspension of [RhCl(coe)$_2$]$_2$ (350 mg, 0.486 mmol) at 273 K. The resulting mixture was stirred at 273 K for 30 min. After that, a toluene solution (3.0 mL) of PH^{t}Bu$_2$ (142 g, 0.972 mmol) at 273 K was added, and the reaction mixture was warmed at room temperature and stirred overnight. The solvent was removed in vacuo, and the residue was washed with pentane (2 × 5 mL) and dried in vacuo to give a yellow powder of **2b** (500 mg, 96%). Anal. Calcd for $C_{22}H_{44}ClNOPRhSi$: calcd: C, 49.30; H, 8.27; N, 2.61. Found: C, 49.50; H, 8.23; N, 2.99. ^{1}H NMR (300 MHz, 298 K, C_6D_6): δ 9.22 (dd, $^{3}J_{H-H} = 6.2$ Hz, $^{4}J_{H-P} = 2.7$ Hz, 1H, py-H^{6}), 6.33 (s, 1H, py-H^{3}), 6.09 (pseudo-d, $^{3}J_{H-H} = 6.2$ Hz, 1H, py-H^{5}), 4.39 (dt, $^{1}J_{H-P} = 329$ Hz, $^{2}J_{H-Rh} \approx {}^{3}J_{H-H} \approx 4.6$ Hz, 1H, PH), 1.56 (s, 3H, CH_3-py), 1.47 (d, $^{3}J_{H-P} = 14.0$ Hz, 18H, P−C(CH_3)$_3$), 1.36 (s, 18H, Si−C(CH_3)$_3$), −18.20 (ddd, $^{1}J_{Rh-H} = 28.8$ Hz, $^{2}J_{P-H} = 19.8$ Hz, $^{3}J_{H-H} = 4.6$ Hz, 1H, Rh−H). ^{13}C{^{1}H} APT plus HSQC ^{1}H−^{13}C (75 MHz, 298 K, C_6D_6): δ 165.8 (m, py-C^{2}), 152.3 (s, py-C^{4}), 148.5 (m, py-C^{6}), 117.8 (dq, $J_{P-C} = 2.6$ Hz, py-C^{5}), 110.8 (m, py-C^{3}), 34.3 (d, $^{1}J_{P-C} = 20.7$ Hz, P−C(CH$_3$)$_3$), 34.2 (m, P−C(CH$_3$)$_3$), 30.5 (s, Si−C(CH$_3$)$_3$), 26.8 (s, Si−C(CH$_3$)$_3$), 20.6 (s, CH$_3$- py). ^{31}P{^{1}H} NMR (121 MHz, 298 K, C_6D_6): δ 58.7 (d, $^{1}J_{\mathrm{P-Rh}} = 142.5$ Hz, Rh−P). ^{29}Si{^{1}H} NMR (60 MHz, 298 K, C_6D_6) plus HMBC ^{1}H−^{29}Si: δ 78.7 ppm (dd, $^{1}J_{\mathrm{Si-Rh}} \approx 30$ Hz, $^{2}J_{\mathrm{Si-P}} \approx 9$ Hz, Rh−Si). HR-MS (ESI$^+$, m/z): calcd for $C_{22}H_{44}NOPRhSi$, $[M - Cl]^+$ 500.1985; found, 500.1839.

Preparation of [Rh(H)(OTf)(κ^2-NSi^{tBu2OPy})(PCy$_3$)] (3a). Toluene (8 mL) was added to a mixture of complex **2a** (0.112 g, 0.163 mmol) and silver triflate (0.042 g, 0.163 mmol) in the dark. The resulting suspension was stirred overnight at room temperature. The yellow solution was filtered through celite, and the solvent was removed in vacuo and washed with pentane (2 × 5 mL). The residue was dried in vacuo to give an off-white powder of **3a** (107 mg, 84%). Anal. Calcd for $C_{33}H_{58}F_3NO_4PRhSSi$: C, 50.57; H, 7.46; N, 1.79. Found: C, 50.73; H, 7.70; N, 1.85. ^{1}H NMR plus HSQC ^{1}H−^{13}C, COSY ^{1}H−^{1}H and NOESY ^{1}H−^{1}H (300 MHz, 298 K, C_6D_6): δ 8.71 (dd, $^{3}J_{H-H} = 6.0$ Hz, $^{4}J_{H-P} = 3.0$ Hz, 1H, py-H^{6}), 6.26 (s, 1H, py-H^{3}), 6.18 (pseudo-d, $^{3}J_{H-H} = 6.0$ Hz, 1H, py-H^{5}), 2.32 (m, 3H, CH-PCy$_3$), 2.14 (m, 3H, CH_2-PCy$_3$), 2.11 (s, 3H, CH$_3$-py), 1.76 (m, 6H, CH_2-PCy$_3$), 1.61 (m, 6H, CH_2-PCy$_3$), 1.56 (s, 9H, CH_3-^{t}Bu), 1.54 (s, 9H, CH_3-^{t}Bu), 1.34 (m, 16H, CH_2-PCy$_3$), −21.72 (dd, $^{1}J_{Rh-H} \approx 33.0$ Hz, $^{2}J_{H-P} \approx 22.0$ Hz, 1H, Rh−H). ^{13}C{^{1}H} APT plus HSQC ^{1}H−^{13}C (75 MHz, 298 K, C_6D_6): δ 164.5 (br, py-C^{2}), 153.5 (s, py-C^{4}), 148.1 (s, py-C^{6}), 118.5 (s, py-C^{5}), 110.9 (s, py-C^{3}), 35.8 (d, $^{1}J_{P-C} = 21.5$ Hz, CH-PCy$_3$), 29.9 (s, 6C, CH$_2$−PCy$_3$), 29.7 (s, 2C, Si−C(CH$_3$)$_3$), 31.0 (s, 6C, CH$_3$-^{t}Bu), 27.7 (d, $^{2}J_{P-C} \approx 10.4$ Hz, 6C, CH$_2$−PCy$_3$), 26.6 (s, 3C, CH$_2$−PCy$_3$), 20.6 (s, CH$_3$-py). ^{31}P{^{1}H} NMR (121 MHz, 298 K, C_6D_6): δ 44.5 (d, $^{1}J_{\mathrm{Rh-P}} \approx 140$ Hz, Rh−P). ^{29}Si{^{1}H} NMR (79 MHz, 298 K, C_6D_6) plus HMBC ^{1}H−^{29}Si: δ 87.9 (dd, $^{1}J_{\mathrm{Rh-Si}} = 40.0$ Hz, $^{2}J_{\mathrm{P-Si}} \approx 9.0$ Hz, Rh−Si). ^{19}F{^{1}H} NMR (282 MHz, 298 K, C_6D_6): δ −77.82 (s, OTf). HR-MS (ESI$^+$, m/z): calcd for $C_{32}H_{58}NOPRhSi$, $[M\text{-}OTf]^+$ 634.3080; found, 634.3155.

Preparation of [Rh(H)(OTf)(κ^2-NSi^{tBu2OPy})(PH^{t}Bu$_2$)] (3b). Toluene (8 mL) was added to a mixture of complex **2b** (100 mg, 0.186 mmol) and silver triflate (48 mg, 0.186 mmol) in the dark. The resulting suspension was stirred overnight at room temperature. A yellow solution was filtered through celite, and the solvent was removed in vacuo. The residue was washed with pentane (2 × 5 mL) and dried in vacuo, at room temperature for 1 h, to give an off-white powder of **3b** (95 mg, 79%). Anal. Calcd for $C_{23}H_{44}F_3NO_4PRhSSi$: C, 42.42; H, 6.83; N, 2.16. Found: C, 42.06; H, 6.76; N, 2.18. ^{1}H NMR (300 MHz, 298 K, C_6D_6): δ 8.72 (dd, $^{3}J_{H-H} = 6.1$ Hz, $^{4}J_{H-P} = 2.9$ Hz 1H, py-H^{6}), 6.25 (s, 1H, py-H^{3}), 6.18 (d, $^{3}J_{H-H} = 6.1$ Hz, 1H, py-H^{5}), 4.10 (dt, $^{1}J_{\mathrm{P-H}} = 340$ Hz; $^{2}J_{H-Rh} = 6.1$ Hz, $^{3}J_{H-H} = 3.9$ Hz, 1H, P−H), 1.55 (s, 3H, CH_3-py), 1.31 (d, $^{3}J_{H-P} = 14.5$ Hz, 18H, P−C(CH_3)$_3$), 1.25 (s, 18H, CH_3-^{t}Bu), −22.18 (ddd, $^{1}J_{Rh-H} = 33.3$ Hz, $^{2}J_{P-H} = 21.5$ Hz, $^{3}J_{H-H} = 3.9$ Hz, 1H, Rh−H). ^{13}C{^{1}H} APT plus HSQC ^{1}H−^{13}C (75 MHz, 298 K, C_6D_6): δ 164.6 (m, py -C^{2}), 153.7 (s, py-C^{4}), 148.1 (d, $^{3}J_{P-H} = 56$ Hz, py-C^{6}), 118.8 (m, py-C^{5}), 111.0 (m, py-C^{3}), 36.4 (m, P−C(CH$_3$)$_3$), 31.8 (m, P−C(CH$_3$)$_3$), 30.6 (s, Si−C(CH$_3$)$_3$), 27.3 (m, P−C(CH$_3$)$_3$), 25.8 (s, Si−C(CH$_3$)$_3$), 20.6 (s, CH$_3$-py). ^{31}P{^{1}H} NMR (121 MHz, 298 K, C_6D_6): δ 55.7 (d, $^{1}J_{\mathrm{P-Rh}} = 141.1$ Hz, Rh−P). ^{29}Si{^{1}H} NMR (60 MHz, 298 K, C_6D_6) plus HMBC ^{1}H−^{29}Si: δ 85.9 (dd, $^{1}J_{\mathrm{Rh-Si}} = 36.1$ Hz, $^{2}J_{\mathrm{P-Si}} \approx 9.0$ Hz, Rh−Si). ^{19}F{^{1}H} NMR (282

MHz, 298 K, C_6D_6): δ −77.6 (s, OTf). HR-MS (ESI$^+$, m/z): calcd for $C_{22}H_{44}NOPRhSi$, $[M - OTf]^+$ 500.1985; found, 500.2089.

Protocol for the Pressurization of Young's NMR Tubes. To pressurize all the samples with hydrogen, the following protocol has been followed: (a) the C_6D_6 solution of the catalyst, the corresponding olefin, and hexamethylbenzene is frozen by carefully introducing the Young's tube in liquid nitrogen; (b) once frozen, the tube is removed from the liquid nitrogen, the argon atmosphere is removed under vacuum, and the desired pressure of hydrogen was introduced; (c) the solution is warmed to room temperature by keeping the tube connected to the hydrogen source at the desired pressure and shaking the tube carefully by hand during the warming up process; (d) the tube is closed, and the solution is frozen again, and the vacuum/H_2 refill process is repeated two more times, so that it is ensured that not only the desired hydrogen pressure is attained but also there are no traces of argon, and the solution is saturated with hydrogen. Below, when it is written "pressurized with", we refer to this protocol.

2a-Catalyzed Reactions of Styrene with 5 bar of H_2 at NMR Scale. 0.089 mmol of styrene (0.010 mL) was added to a Young's NMR tube containing a solution of **2a** (3 mg, 0.0045 mmol) and hexamethylbenzene (7.20 mg, 0.045 mmol) in C_6D_6 (0.5 mL). The resulting solution was pressurized with H_2 (5 bar) and heated at 353 K and monitored by ^1H NMR.

3a-Catalyzed Reactions of Alkenes with 5 bar of H_2 at NMR Scale. 0.076 mmol of the corresponding alkene (styrene, 0.009 mL; 2-methylstyrene, 0.010 mL; 3-methylstyrene, 0.010 mL; *cis*-cyclooctene, 0.010 mL; 1 pentene, 0.008 mL; *cis*-2-pentene, 0.008 mL; methyl acrylate, 0.007 mL; 4-pentenoic acid, 0.008 mL) was added to a Young's NMR tube containing a solution of **3a** (3 mg, 0.0038 mmol) and hexamethylbenzene (6.20 mg, 0.038 mmol) in C_6D_6 (0.5 mL). The resulting solution was pressurized with H_2 (5 bar) and heated at 353 K and monitored by ^1H NMR.

2b-Catalyzed Reactions of Styrene with 5 bar of H_2 at NMR Scale. 0.11 mmol of the styrene (0.013 mL) was added to a Young's NMR tube containing a solution of **2b** (3 mg, 0.0056 mmol) and hexamethylbenzene (9.00 mg, 0.056 mmol) C_6D_6 (0.5 mL). The resulting solution was pressurized with H_2 (5 bar) and heated at 353 K and monitored by ^1H NMR.

3b-Catalyzed Reactions of Alkenes with 5 bar of H_2 at NMR Scale. 0.092 mmol of the corresponding alkene (styrene, 0.011 mL; 2-methylstyrene, 0.012 mL; 3-methylstyrene, 0.012 mL; *cis*-cyclooctene, 0.012 mL; 1 pentene, 0.010 mL; *cis*-2-pentene, 0.010 mL; methyl acrylate, 0.0095 mL; 4-pentenoic acid, 0.008 mL) was added to a Young's NMR tube containing a solution of **3b** (3 mg, 0.0046 mmol) and hexamethylbenzene (7.50 mg, 0.046 mmol) in C_6D_6 (0.5 mL). The resulting solution was pressurized with H_2 (5 bar) and heated at 353 K and monitored by ^1H NMR.

4a-Catalyzed Reactions of Styrene with 5 bar of H_2 at NMR Scale. 0.069 mmol of the styrene (0.008 mL) was added to a Young's NMR tube containing a solution of **4a** (3 mg, 0.0034 mmol) and hexamethylbenzene (5.60 mg, 0.034 mmol) in C_6D_6 (0.5 mL). The resulting solution was pressurized with H_2 (5 bar) and heated at 353 K and monitored by ^1H NMR.

4b-Catalyzed Reactions of Styrene with 5 bar of H_2 at NMR Scale. 0.081 mmol of the styrene (0.009 mL) was added to a Young's NMR tube containing a solution of **4b** (3 mg, 0.0041 mmol) and hexamethylbenzene (6.60 mg, 0.041 mmol) in C_6D_6 (0.5 mL). The resulting solution was pressurized with H_2 (5 bar) and heated at 353 K and monitored by ^1H NMR.

Single-Crystal Structure Determination. Single crystals suitable for X-ray diffraction were obtained by slow cooling (5 °C) of pentane (5 mL) saturated solutions of the corresponding complex.

X-ray diffraction data of compound **2a** were collected in the XALOC beamline at ALBA synchrotron (Spain),[27] at 100 K with 0.729740 Å wavelength, using a Dectris Pilatus 6 M detector placed at 122.1 mm from the crystal. Intensity transmission was attenuated to 50%. A complete φ scan was recorded with a 0.3° and 0.1 s per frame rotation step. To ensure better redundancy, another complete φ scan was recorded with the same crystal mounted in a different orientation. Both data sets were integrated and corrected from absorption effects with XIA2 program[28−30] and subsequently scaled with SORTAV program.[31] X-ray diffraction data of compounds **2b** and **3a** were collected on a VENTURE Bruker diffractometer, using Mo κ_α (λ = 0.71073 Å). Single crystals were mounted on a MiTeGen support and cooled to 100(2) K with open-flow nitrogen gas. Data were collected using ω and φ scans with narrow frames strategies. Diffracted intensities of **2b** and **3a** were integrated and corrected from absorption effects with APEX4 package.[32] Crystal structures were solved and refined using SHELXS[33] and SHELXL[34] included in Olex2 program.[35] Special refinement details have been reported below.

CCDC 2280466−2280468 contain the supplementary crystallographic data for this paper. These data can be obtained free of charge from the Cambridge Crystallographic Data Center via www.ccdc.cam.ac.uk/data_request/cif.

*Crystal Data of **2a**.* $C_{32}H_{58}ClNOPRhSi$; M_r = 670.21; yellow prism 0.005 × 0.005 × 0.120 mm^3; monoclinic $P2_1/c$; a = 14.27470(10) Å, b = 11.38320(10) Å; c = 21.0193(2) Å, b = 92.1060(10)°; V = 3413.16(5) Å^3; Z = 4; D_c = 1.304 g/cm^3; μ = 0.725 mm^{-1}; min and max absorption correction factors: 0.9759 and 1.0; $2\theta_{max}$ = 67.102°; 115,994 reflections measured, 11,267 unique; R_{int} = 0.1348; number of data/restraint/parameters: 11,267/0/351; R_1 = 0.0690 [10,825 reflections, $I > 2\sigma(I)$], w$R(F^2)$ = 0.1721 (all data); largest difference peak: 2.436 e Å^{-3}. The highest residual density peaks are found close to the metal atom. Hydride ligand position was calculated with the HYDEX program.[36] Its isotropic atomic displacement parameter has been constrained to be 1.5 times the equivalent isotropic *adp* of the metal atom.

*Crystal Data of **2b**.* $C_{22}H_{44}ClNOPRhSi$; M_r = 536.00; yellow prism 0.100 × 0.118 × 0.190 mm^3; monoclinic $P2_1/n$; a = 8.8119(3) Å, b = 10.5412(7) Å; c = 28.8510(19) Å, b = 98.570(2)°; V = 2650.0(3) Å^3; Z = 4; D_c = 1.343 g/cm^3; μ = 0.863 mm^{-1}; min and max absorption correction factors: 0.6947 and 0.7467; $2\theta_{max}$ = 56.554°; 110,389 reflections measured, 6533 unique; R_{int} = 0.0309; number of data/restraint/parameters: 6533/0/273; R_1 = 0.0180 [6403 reflections, $I > 2\sigma(I)$], w$R(F^2)$ = 0.0476 (all data); largest difference peak: 0.589 e Å^{-3}. Hydride and hydrogen atoms of the P−H fragment have been included in the model in observed positions and as freely refined.

*Crystal Data of **3a**.* $C_{33}H_{58}F_3NO_4PRhSSi$; M_r = 783.83; yellow prism 0.100 × 0.170 × 0.200 mm^3; monoclinic $C2/c$; a = 19.6141(13) Å, b = 15.2804(10) Å; c = 26.080(2) Å, b = 110.343(2)°; V = 7329.0(9) Å^3; Z = 8; D_c = 1.421 g/cm^3; μ = 0.651 mm^{-1}; min and max. absorption correction factors: 0.8624 and 0.9282; $2\theta_{max}$ = 72.774°; 161,885 reflections measured, 17,751 unique; R_{int} = 0.0295; number of data/restraint/parameters: 17,751/0/417; R_1 = 0.0258 [16,521 reflections, $I > 2\sigma(I)$], w$R(F^2)$ = 0.0609 (all data); largest difference peak: 1.164 e Å^{-3}. Hydride ligand has been included in the model in observed position and as freely refined.

■ ASSOCIATED CONTENT

Supporting Information

The Supporting Information is available free of charge at https://pubs.acs.org/doi/10.1021/acs.organomet.3c00498.

Additional experimental details, NMR data, and methods and computational details (PDF)

Cartesian coordinates of computed structures (XYZ)

Accession Codes

CCDC 2280466−2280468 contain the supplementary crystallographic data for this paper. These data can be obtained free of charge via www.ccdc.cam.ac.uk/data_request/cif, or by emailing data_request@ccdc.cam.ac.uk, or by contacting The Cambridge Crystallographic Data Centre, 12 Union Road, Cambridge CB2 1EZ, UK; fax: +44 1223 336033.

■ AUTHOR INFORMATION

Corresponding Authors

Israel Fernández − *Departamento de Química Orgánica I and Centro de Innovación en Química Avanzada, Facultad de Ciencias Químicas, Universidad Complutense de Madrid, 28040 Madrid, Spain;* orcid.org/0000-0002-0186-9774; Email: israel@quim.ucm.es

Francisco J. Fernández-Álvarez − *Departamento de Química Inorgánica-Instituto de Síntesis Química y Catálisis Homogénea (ISQCH), Universidad de Zaragoza—CSIC, 50009 Zaragoza, Spain;* orcid.org/0000-0002-0497-1969; Email: paco@unizar.es

Authors

Alejandra Gómez-España − *Departamento de Química Inorgánica-Instituto de Síntesis Química y Catálisis Homogénea (ISQCH), Universidad de Zaragoza—CSIC, 50009 Zaragoza, Spain; Universidad Pedagógica Nacional Francisco Morazán-UPNFM, 11101 Tegucigalpa, Honduras*

Pilar García-Orduña − *Departamento de Química Inorgánica-Instituto de Síntesis Química y Catálisis Homogénea (ISQCH), Universidad de Zaragoza—CSIC, 50009 Zaragoza, Spain*

Fernando J. Lahoz − *Departamento de Química Inorgánica-Instituto de Síntesis Química y Catálisis Homogénea (ISQCH), Universidad de Zaragoza—CSIC, 50009 Zaragoza, Spain;* orcid.org/0000-0001-8054-2237

Complete contact information is available at:
https://pubs.acs.org/10.1021/acs.organomet.3c00498

Author Contributions

The manuscript was written through contributions of all authors. All authors have given approval to the final version of the manuscript.

Notes

The authors declare no competing financial interest.
Computational details: see the Supporting Information for computational details.

■ ACKNOWLEDGMENTS

The support from the Spanish MCIN/AEI/10.13039/501100011033 (grants PID2019-106184GB-I00, RED2018-102387-T and PID2022-139318NB-I00 to I.F.; and PGC2018-099383−B-I00 and PID-1262120B-I00 to FJFA) and Aragón Goverment (grant E42_23R) is gratefully acknowledged. A. G.-E. thankfully acknowledges the Universidad de Zaragoza and Banco Santander for a predoctoral fellowship "Ayudas para iberoamericanos y ecuatoguineanos en Estudios de Doctorado. Universidad de Zaragoza—Santander Universidades (2022−2023)". Some X-ray diffraction experiments were performed at XALOC beamline at ALBA synchrotron with the collaboration of ALBA staff.

■ REFERENCES

(1) Selected reviews: (a) Cabeza, J. A.; García-Álvarez, P. Tetralenes *versus* tetrylenes as precursors to transition metal complexes featuring tridentate PEP tetryl ligands (E = Si, Ge, Sn). *Chem.—Eur. J.* **2023**, *29*, No. e202203096. (b) Komuro, T.; Nakajima, Y.; Takaya, J.; Hashimoto, H. Recent progress in transition metal complexes supported by multidentate ligands featuring group 13 and 14 elements as coordinating atoms. *Coord. Chem. Rev.* **2022**, *473*, 214837. (c) Whited, M. T. Pincer-supported metal/main-group bonds as platforms for cooperative transformations. *Dalton Trans.* **2021**, *50*, 16443−16450. (d) Whited, M. T.; Zhang, J.; Ma, S.; Nguyen, B. D.; Janzen, D. E. Silylene-assisted hydride transfer to CO$_2$ and CS$_2$ at a [P$_2$Si]Ru pincer-type complex. *Dalton Trans.* **2017**, *46*, 14757−14761. (e) Simon, M.; Breher, F. Multidentate silyl ligands in transition metal chemistry. *Dalton Trans.* **2017**, *46*, 7976−7997. (f) Balakrishna, M. S.; Chandrasekaran, P.; George, P. P. Silicon based phosphines with P_Si_P, P_C_Si_C_P and P_O_Si_O_P linkages and their coordination chemistry and catalytic applications. *Coord. Chem. Rev.* **2003**, *241*, 87−117.

(2) (a) Tanabe, M.; Osakada, K. Transition Metal Complexes of Silicon (Excluding Silylene Complexes), Chapter 2. In *Organosilicon Compounds, Theory and Experiment (Synthesis)*; Lee, V. Y., Ed.; Academic Press: London, 2017. (b) Sola, E. Silicon-based pincers: *trans* influence and functionality, Chapter 19. In *Pincer Compounds: Chemistry and Applications*; Morales-Morales, D., Ed.; Elsevier: Amsterdam, 2018. (c) Turculet, L. PSiP transition-metal pincer complexes: synthesis, bond activation, and catalysis, Chapter 6. In *Pincer and Pincer-Type Complexes: Applications in Organic Synthesis and Catalysis*, 1st ed.; Szabó, K. J.; Wendt, O. F., Eds.; John Willey and Sons, 2014.

(3) (a) Yang, B.; Tan, X.; Ge, Y.; Li, Y.; He, C. Stereodivergent asymmetric synthesis of P-atropisomeric Si-stereogenic monohydrosilanes. *Org. Chem. Front.* **2023**, *10*, 4862−4870. (b) Yang, B.; Gao, J.; Tan, X.; Ge, Y.; He, C. Chiral PSiSi-Ligand Enabled Iridium-Catalyzed Atroposelective Intermolecular C−H Silylation. *Angew. Chem., Int. Ed.* **2023**, *62*, No. e202307812. (c) Shen, J.; Usui, R.; Sunada, Y. An Iridium Complex with a Phosphine-Pendant Silyl Ligand as an Efficient Catalyst for the (*E*)-Selective Semihydrogenation of Alkynes. *Eur. J. Org Chem.* **2022**, *2022*, No. e202101563. (d) Park, S.; Kim, B. G.; Göttker-Schnetmann, I.; Brookhart, M. Redistribution of Trialkyl Silanes Catalyzed by Iridium Silyl Complexes. *ACS Catal.* **2012**, *2*, 307−316. (e) García-Camprubi, A.; Martin, M.; Sola, E. Addition of Water Across Si-Ir Bonds in Iridium Complexes with K-P,P,Si (biPSi)Pincer Ligands. *Inorg. Chem.* **2010**, *49*, 10649−11065. (f) Montiel-Palma, V.; Piechaczyk, O.; Picot, A.; Auffrant, A.; Vendier, L.; Le Floch, P.; Sabo-Etienne, S. Bonding Mode of a Bifunctional P ∼ Si-H Ligand in the Ruthenium Complex "Ru(PPh$_2$CH$_2$OSiMe$_2$H)$_3$. *Inorg. Chem.* **2008**, *47*, 8601−8603. (g) Clark, G. R.; Lu, G.-L.; Rickard, C. E. F.; Roper, W. R.; Wright, L. J. Metallacyclic complexes with *ortho*-silylated triphenylphosphine ligands, L$_n$Os(κ^2(*Si,P*)-SiMe$_2$C$_6$H$_4$PPh$_2$), derived from thermal reactions of the coordinatively unsaturated trimethylsilyl, methyl complex, Os(SiMe$_3$)(Me)(CO)(PPh$_3$)$_2$. *J. Organomet. Chem.* **2005**, *690*, 3309−3320. (h) Lee, Y.-J.; Lee, J.-D.; Kim, S. J.; Keum, S.; Ko, J.; Suh, I.-H.; Cheong, M.; Kang, S. O. Synthesis, Structure, and DFT Calculation of (Phosphino-*o*-carboranyl)silyl Group 10 Metal Complexes: Formation of Stable *trans*-Bis(*P,Si*-chelate)metal Complexes. *Organometallics* **2004**, *23*, 203−214. (i) Okazaki, M.; Ohshitanai, S.; Iwata, M.; Tobita, H.; Ogino, H. Synthesis and reactivity of (phosphinoaklyl)silyl complexes. *Coord. Chem. Rev.* **2002**, *226*, 167−178.

(4) (a) Wagler, J.; Gericke, R. Pd−Si complexes of the type ClPd(μ2 -pyO)4SiR (R = Me, Ph, Bn, Allyl, κO-(pyO)PdCl(η3 -allyl); pyO = pyridine-2-olate): The influence of substituent R on the Pd−Si bond. *Polyhedron* **2023**, *245*, 116663. (b) Ehrlich, L.; Gericke, R.; Brendler, E.; Wagler, J. (2-Pyridyloxy)silanes as Ligands in Transition Metal Coordination Chemistry. *Inorganics* **2018**, *6*, 119. (c) Fernández-Alvarez, F. J.; Lalrempuia, R.; Oro, L. A. Monoanionic NSiN-type ligands in transition metal coordination chemistry and catalysis. *Coord. Chem. Rev.* **2017**, *350*, 49−60.

(5) (a) Ouyang, Z.; Deng, L. Iron(II) Complexes Featuring Bidentate N-Heterocyclic Carbene−Silyl Ligands: Synthesis and Characterization. *Organometallics* **2013**, *32*, 7268−7271. (b) Mo, Z.; Liu, Y.; Deng, L. Anchoring of Silyl Donors on a N-Heterocyclic Carbene through the Cobalt-Mediated Silylation of Benzylic C-H Bonds. *Angew. Chem., Int. Ed.* **2013**, *52*, 10845−10849. (c) Deng, L.; Mo, Z. Post-Functionalization: A Useful Method for the Synthesis of Donor-Functionalized N-Heterocyclic Carbene−Transition-Metal Catalysts. *Synlett* **2014**, *25*, 1045−1049. (d) Sun, J.; Ou, C.; Wang,

C.; Uchiyama, M.; Deng, L. Silane-Functionalized N-Heterocyclic Carbene−Cobalt Complexes Containing a Five-Coordinate Silicon with a Covalent Co−Si Bond. *Organometallics* **2015**, *34*, 1546−1551. (e) Sun, J.; Luo, L.; Luo, Y.; Deng, L. An NHC−Silyl−NHC Pincer Ligand for the Oxidative Addition of C−H, N−H, and O−H Bonds to Cobalt(I) Complexes. *Angew. Chem., Int. Ed.* **2017**, *56*, 2720−2724.

(6) (a) Almenara, N.; Garralda, M. A.; Lopez, X.; Matxain, J. M.; Freixa, Z.; Huertos, M. A. Hydrogen Tunneling in Catalytic Hydrolysis and Alcoholysis of Silanes. *Angew. Chem., Int. Ed.* **2022**, *61*, No. e202204558. (b) Azpeitia, S.; Martínez-Martínez, A. J.; Garralda, M. A.; Weller, A. S.; Huertos, M. A. Si−C(sp3) bond activation through oxidative addition at a Rh(I) centre. *Dalton Trans.* **2020**, *49*, 5416−5419. (c) Almenara, N.; Miranda, J. I.; Rodríguez-Diéguez, A.; Garralda, M. A.; Huertos, M. A. A phosphine-stabilized silylene rhodium complex. *Dalton Trans.* **2019**, *48*, 17179−17183. (d) Azpeitia, S.; Rodriguez-Dieguez, A.; Garralda, M. A.; Huertos, M. A. From remote alkenes to linear silanes or allylsilanes depending on the metal center. *ChemCatChem* **2018**, *10*, 2210−2213. (e) Azpeitia, S.; Prieto, U.; San Sebastián, E.; Rodríguez-Diéguez, A.; Garralda, M. A.; Huertos, M. A. Alkene-alkyl interconversion: an experimental and computational study of the olefin insertion and β-hydride elimination processes. *Dalton Trans.* **2018**, *47*, 6808−6818.

(7) (a) Prieto, U.; Azpeitia, S.; Sebastian, E. S.; Freixa, Z.; Garralda, M. A.; Huertos, M. A. Steric Effects in the Catalytic Tandem Isomerization-Hydrosilylation Reaction. *ChemCatChem* **2021**, *13*, 1403−1409. (b) Almenara, N.; Azpeitia, S.; Garralda, M. A.; Huertos, M. A. Rh(III)-Catalysed solvent-free hydrodehalogenation of alkyl halides by tertiary silanes. *Dalton Trans.* **2018**, *47*, 16225−16231. (c) Azpeitia, S.; Fernández, B.; Garralda, M. A.; Huertos, M. A. Silyl-Thioether Multidentate Ligands - Synthesis of Rh^{III} Complexes via Rh^{I}/Rh^{III} Mixed-Valent and Cyclooctenyl Intermediates. *Eur. J. Inorg. Chem.* **2015**, *2015*, 5451−5456.

(8) (a) Guzmán, J.; García-Orduña, P.; Polo, V.; Lahoz, F. J.; Oro, L. A.; Fernández-Alvarez, F. J. Ir-catalyzed selective reduction of CO_2 to the methoxy or formate level with $HSiMe(OSiMe_3)_2$. *Catal. Sci. Technol.* **2019**, *9*, 2858−2867. (b) Guzmán, J.; García-Orduña, P.; Lahoz, F. J.; Fernández-Alvarez, F. J. Unprecedent formation of methylsilylcarbonates from iridium-catalyzed reduction of CO_2 with hydrosilanes. *RSC Adv.* **2020**, *10*, 9582−9586. (c) Guzmán, J.; Urriolabeitia, A.; Polo, V.; Fernández-Buenestado, M.; Iglesias, M.; Fernández-Alvarez, F. J. Dehydrogenation of formic acid using iridium-NSi species as catalyst precursors. *Dalton Trans.* **2022**, *51*, 4386−4393. (d) Guzmán, J.; Urriolabeitia, A.; Padilla, M.; García-Orduña, P.; Polo, V.; Fernández-Alvarez, F. J. Mechanism insights into the iridium(III)- and $B(C_6F_5)_3$-catalyzed reduction of CO_2 to the formaldehyde level with tertiary silanes. *Inorg. Chem.* **2022**, *61*, 20216−20221.

(9) For examples of Mo- and W-κ^2-(NSi) species see: Kanno, Y.; Komuro, T.; Tobita, H. Direct conversion of a Si-C(aryl) bond to Si-heteroatom bonds in the reactions of η^3-α-silabenzyl molybdenum and tungsten complexes with 2-substituted pyridines. *Organometallics* **2015**, *34*, 3699−3705.

(10) For examples of Fe-κ^2-(NSi) species see: (a) Sato, T.; Okazaki, M.; Tobita, H. Alkoxyhydrosilanes as sources of silylene ligands: novel approaches to transition metal-silylene complexes. *Chem. Lett.* **2004**, *33*, 868−869. (b) Sato, T.; Okazaki, M.; Tobita, H.; Ogino, H. Synthesis, structure, and reactivity of novel iron(II) complexes with a five-membered chelate ligand $\kappa^2(Si,N)$-$SiMe_2O(2\text{-}C_5H_4N)$. *J. Organomet. Chem.* **2003**, *669*, 189−199. (c) Tobita, H.; Sato, T.; Okazaki, M.; Ogino, H. Synthesis and structures of bis(silylene)iron complexes containing new six-membered chelate rings. *J. Organomet. Chem.* **2000**, *611*, 314−322.

(11) For examples of Ru-κ^2-(NSi) species see: Kwok, W.-H.; Lu, G.-L.; Rickard, C. E. F.; Roper, W. R.; Wright, L. J. Tethered silyl complexes from nucleophilic substitution reactions at the Si-Cl bond of the chloro(diphenyl)silyl ligand in $Ru(SiClPh_2)(\kappa^2\text{-}S_2CNMe_2)(CO)(PPh_3)_2$. *J. Organomet. Chem.* **2004**, *689*, 2979−2987.

(12) Guzmán, J.; Bernal, A. M.; García-Orduña, P.; Lahoz, F. J.; Polo, V.; Fernández-Alvarez, F. J. 2-Pyridone-stabilized iridium silylene/silyl complexes: structure and QTAIM analysis. *Dalton Trans.* **2020**, *49*, 17665−17673.

(13) García-Orduña, P.; Fernández, I.; Oro, L. A.; Fernández-Alvarez, F. J. Origin of the Ir-Si bond shortening in Ir-NSiN complexes. *Dalton Trans.* **2021**, *50*, 5951−5959.

(14) Gómez-España, A.; García-Orduña, P.; Guzmán, J.; Fernández, I.; Fernández-Alvarez, F. J. Synthesis and characterization of Ir-(κ^2-NSi) species active toward the solventless hydrolysis of $HSiMe(OSiMe_3)_2$. *Inorg. Chem.* **2022**, *61*, 16282−16294.

(15) (a) Guzmán, J.; Bernal, A. M.; García-Orduña, P.; Lahoz, F. J.; Oro, L. A.; Fernández-Alvarez, F. J. Selective reduction of formamides to *O*-silylated hemiaminals or methylamines with $HSiMe_2Ph$ catalyzed by iridium complexes. *Dalton Trans.* **2019**, *48*, 4255−4262. (b) Gomez-España, A.; Lopez-Morales, J. L.; Español-Sanchez, B.; García-Orduña, P.; Lahoz, F. J.; Iglesias, M.; Fernández-Alvarez, F. J. Iridium-(κ^2-NSi) catalyzed dehydrogenation of formic acid: effect of auxiliary ligands on the catalytic performance. *Dalton Trans.* **2023**, *52*, 6722−6729. (c) Gomez-España, A.; Lopez-Morales, J. L.; Español-Sanchez, B.; García-Orduña, P.; Lahoz, F. J.; Iglesias, M.; Fernández-Alvarez, F. J. Correction: Iridium-(κ^2-NSi) catalyzed dehydrogenation of formic acid: effect of auxiliary ligands on the catalytic performance. *Dalton Trans.* **2023**, *52*, 11361−11362.

(16) Guzmán, J.; Torguet, A.; García-Orduña, P.; Lahoz, F. J.; Oro, L. A.; Fernández-Alvarez, F. J. Rhodium-catalyzed formation of silylcarbamates from the reaction of secondary amines with CO_2 and hydrosilanes. *J. Organomet. Chem.* **2019**, *897*, 50−56.

(17) (a) Prieto-Pascual, U.; Rodríguez-Diéguez, A.; Freixa, Z.; Huertos, M. A. Tailor-made synthesis of hydrosilanols, hydrosiloxanes, and silanediols catalyzed by di-silyl rhodium(III) and iridium(III) complexes. *Inorg. Chem.* **2023**, *62*, 3095−3105. (b) Prieto-Pascual, U.; Martínez de Morentin, A.; Choquesillo-Lazarte, D.; Rodríguez-Diéguez, A.; Freixa, Z.; Huertos, M. A. Catalytic activation of remote alkenes through silyl-rhodium(III) complexes. *Dalton Trans.* **2023**, *52*, 9090−9096.

(18) Sato, K.; Komuro, T.; Hashimoto, H.; Tobita, H. Bifunctional Rhodium Complex Featuring a Silyl-1,8-naphthyridine *Si,N*-Chelate Ligand: Cooperation of Metal and Pendant Base for capture and Bond-weakening of BH_3. *Chem. Lett.* **2020**, *49*, 1431−1434.

(19) Corey, J. Y.; Braddock-Wilking, J. Reactions of hydrosilanes with transition-metal complexes: formation of stable transition-metal silyl compounds. *Chem. Rev.* **1999**, *99*, 175−292.

(20) Addison, A. W.; Rao, T. N.; Reedijk, J.; van Rijn, J.; Verschoor, G. C. Synthesis, structure, and spectroscopic properties of copper(II) compounds containing nitrogen−sulphur donor ligands; the crystal and molecular structure of aqua[1,7-bis(N-methylbenzimidazol-2′-yl)-2,6-dithiaheptane]copper(II) perchlorate. *J. Chem. Soc., Dalton Trans.* **1984**, 1349−1356.

(21) (a) Whited, M. T.; Trenerry, M. J.; DeMeulenaere, K. E.; Taylor, B. L. H. Computational and experimental investigation of alkene hydrogenation by pincer-type $[P_2Si]Rh$ complex: alkane release via competitive σ-bond metathesis and reductive elimination. *Organometallics* **2019**, *38*, 1493−1501. (b) Whited, M. T.; Deetz, A. M.; Donnell, T. M.; Janzen, D. E. Examining the role of Rh/Si cooperation in alkene hydrogenation by a pincer-type $[P_2Si]Rh$ complex. *Dalton Trans.* **2016**, *45*, 9758−9761.

(22) Sato, K.; Komuro, T.; Osawa, T.; Hashimoto, H.; Tobita, H. Iridium Complexes with a Naphthyridine-Based *Si,N*-Ligand: Synthesis and Catalytic Activity toward Olefin Hydrogenation. *Organometallics* **2022**, *41*, 2612−2621.

(23) Fernández-Alvarez, F. J.; Polo, V.; García-Orduña, P.; Lahoz, F. J.; Pérez-Torrente, J. J.; Oro, L. A.; Lalrempuia, R. Synthesis and Reactivity at the Ir-MeTpm Platform: From κ^1-N Coordination to κ^3-N- based Organometallic Chemistry. *Dalton Trans.* **2019**, *48*, 6455−6463.

(24) Nelsen, E. R.; Landis, C. R. Interception and characterization of alkyl and acyl complexes in rhodium-catalyzed hydroformylation of styrene. *J. Am. Chem. Soc.* **2013**, *135*, 9636−9639.

(25) Perutz, R. N.; Sabo-Etienne, S. The σ-CAM Mechanism: σ Complexes as the Basis of σ-Bond Metathesis at Late-Transition-Metal Centers. *Angew. Chem., Int. Ed.* **2007**, *46*, 2578−2592.

(26) (a) van der Ent, A.; Onderdelinden, A. L.; Schunn, R. A. Chlorobis(cyclooctene)rhodium(I) and Iridium(I) complexes. *Inorg. Synth.* **1973**, *14*, 92−95. (b) van der Ent, A.; Onderdelinden, A. L.; Schunn, R. A. Chlorobis(Cyclooctene)Rhodium(I) and-Iridium(I) complexes. *Inorg. Synth.* **1990**, *28*, 90−92.

(27) Juanhuix, J.; Gil-Ortiz, F.; Cuní, G.; Colldelram, C.; Nicolás, J.; Lidón, J.; Boter, E.; Ruget, C.; Ferrer, S.; Benach, J. Developments in optics and performance at BL-13 XALOC, the macromolecular crystallography beamline at the Alba Synchrotron. *J. Synchrotron Radiat.* **2014**, *21*, 679−689.

(28) Winter, G.; Waterman, D. G.; Parkhurst, J. M.; Brewster, A. S.; Gildea, R. J.; Gerstel, M.; Fuentes-Montero, L.; Vollmar, M.; Michels-Clark, T.; Young, I. D.; Sauter, N. K.; Evans, G. DIALS: implementation and evaluation of a new integration package. *Acta Crystallogr.* **2018**, *74*, 85−97.

(29) Evans, P. Scaling and assessment of data quality. *Acta Crystallogr.* **2006**, *62*, 72−82.

(30) Grosse-Kunstleve, R. W.; Sauter, N. K.; Moriarty, N. W.; Adams, P. D. The computational crystallography toolbox: crystallographic algorithms in a reusable software framework. *J. Appl. Crystallogr.* **2002**, *35*, 126−136.

(31) Blessing, R. H. Data Reduction and Error Analysis for Accurate Single Crystal Diffraction Intensities. *Crystallogr. Rev.* **1987**, *1*, 3−58.

(32) *APEX 4 v2021.10-0*; Bruker AXS.

(33) Sheldrick, G. M. A short history of SHELX. *Acta Crystallogr.* **2008**, *64*, 112−122.

(34) Sheldrick, G. M. Crystal structure refinement with SHELXL. *Acta Crystallogr.* **2015**, *71*, 3−8.

(35) Dolomanov, O. V.; Bourhis, L. J.; Gildea, R. J.; Howard, J. A. K.; Puschmann, H. OLEX2: A complete structure solution, refinement and analysis program. *J. Appl. Crystallogr.* **2009**, *42*, 339−341.

(36) Orpen, A. G. Indirect location of hydride ligands in metal cluster complexes. *J. Chem. Soc., Dalton Trans.* **1980**, 2509−2516.